applied sciences

MDPI

Article

CNT-Coated Quartz Woven Fabric Electrodes for Robust Lithium-ion Structural Batteries

Mi-Young Park [1], Chun-Gon Kim [1,*] and Joo-Hyung Kim [2,*]

[1] Department of Aerospace Engineering, Korea Advanced Institute of Science and Technology, Daejeon 34141, Korea; doriangray@kaist.ac.kr
[2] School of Materials Science and Engineering, Gyeongsang National University, Jinju 52828, Korea
* Correspondence: cgkim@kaist.edu (C.-G.K.); kimjoohyung@gnu.ac.kr (J.-H.K.)

Received: 13 November 2020; Accepted: 1 December 2020; Published: 2 December 2020

Abstract: Reliability in various conditions for Li-ion batteries has been considered one of the most important factors when determining usability. Silica-based fabric has great potential to be an alternative material for electrode support, providing mechanical and physical stability in lithium-ion batteries. In this study, a carbon nanotube (CNT)-coated quartz woven fabric electrode (C-QWF) with impressive electrochemical characteristics was synthesized via a sequential two-step deposition process using Al and Fe as metal catalyst and CH_4 as a carbon source. The C-QWF electrode exhibited a considerable specific discharge capacity of 369 mAh g^{-1} at a rate of 0.1 C-rate after cycling. The battery cell showed self-recovering ability during the cycling test at 1 C-rate, although the silica fabric has sluggish electrical conductivity. The C-QWF electrode has a superior electrochemical performance, providing new perspectives on textile fabric electrodes for robust Li-ion batteries, especially load-bearing structural batteries.

Keywords: carbon nanotubes; plasma-enhanced chemical vapor deposition; quartz woven fabric; lithium-ion batteries

1. Introduction

While energy technology has been intensively researched to meet the rapidly increasing energy demand around the world for the past 20 years, demand is increasing explosively for industrial energy as can be seen in the popularity of consumer portable electronics, wireless transmission, vehicle control system, uninterrupted power supply, and backup power and pulse, all of which require high economic efficiency [1–3]. As unmanned vehicle technology is actively applied industrially for the purpose of intelligent and economic operation of vehicles, the need for an optimal system for increasing the amount of onboard equipment and reducing the weight of the vehicle is also required. The demand for a breakthrough to overcome the limitation of conventional lithium-ion batteries (LIBs) has been accelerating [4]. On the other hand, eco-friendly policies, such as reducing carbon dioxide emissions related to global warming, have become hot topics in the traditional automobile industry, which generates a lot of smoke. Many efforts are being made to commercialize technologies in various fields for electric vehicles. This trend has seen the rise of energy-efficient transportation means based on economic feasibility. As such, there has been an increase in demand for reducing fuel economy, extending operating distance, and expertise for advanced system integration in fields such as the automobile and aerospace industries. To save costs in the energy efficiency of a vehicle, there have been attempts to increase the operating efficiency by reducing the weight of parts, or increasing the energy generation per unit weight by increasing the specific capacity of the battery required for the system. In line with this approach, various studies have been actively conducted in the last 20 years, particularly in the US and Europe. It is a concept that improves energy efficiency at the system level as

a study on a multifunctional structure that can store and release energy while maintaining the structural materials' mechanical performance using fiber composites [5–8]. Through weight reduction that maintains the strength of the structure, a space that can perform more functions or tasks in the same volume is obtained. At the same time, this space is used as an energy storage electrode, increasing the energy efficiency of the entire system. Eventually, from the perspective of the energy system, it is expected that the development of excellent energy efficiency will be possible through the correlation between mechanical strength and electrochemical performance [9,10].

The most common fiber types in composites are glass and carbon, which can contribute to electrode support in a structural battery [11–14]. There are some conflicting requirements in the electrode support. The continuity in the load path is required from an electric energy storage portion to the adjacent structure portion for the structural function, while the discontinuity in the electrical path is essential between these two portions of electrode support for proper battery function. In this regard, a glass fabric such as quartz woven fabric (QWF) is a better choice for electrode support if the fabric is modified in the energy storage portion by Li-storable and electric-conducting materials like carbon nanotube (CNT) forest. Silica, used as a fiber woven fabric, is a good candidate material, but still needs a 3D network shape that can provide continuous electron transport paths with adequate levels of electrical conduction. To date, the research has reported the performance of structural supercapacitors with potential applications, and the research on structural cells is at a basic stage that hardly deviates from conventional approaches [15,16]. Research on a multifunctional robust battery to utilize the excellent mechanical and electrical properties of the composite material can suggest a new energy storage paradigm that can improve energy efficiency in various systems requiring mechanical strength. Furthermore, it is expected to present a new perspective that can ultimately be expanded to the field of high-efficiency energy storage complex system technology, especially since the system can be combined [17–20].

2. Materials and Methods

Carbon Nanotube Growth on Quartz Woven Fabric: For the confirmation of the two nanostructure-coated electrodes, CNT was grown on the quartz woven fabric via a plasma-enhanced chemical vapor deposition (PECVD). Nanoparticles were deposited via sequential steps on the woven fabric, with the Al layer functioning as a buffer, and the Fe-catalyst layer activating CNT growth. The pressure of the evaporation chamber was kept under 2×10^{-6} Torr to prevent the oxidation of the Al layer. The metal catalysts ware successfully fabricated without breaking the vacuum pressure. The CNT growth on quartz in the PECVD chamber was carried out at 600-700 °C for 30 min with a flow of 100 sccm CH_4 as a carbon source and 10 sccm of H_2. The process was maintained with 320 W at a pressure of 800 mTorr, with a 13.75 MHz RF plasma as an extra energy source to enhance growth of vertically aligned CNTs.

Material Characterization: The X-ray diffraction pattern is confirmed by X-ray diffraction (XRD, D/MAX-RB 12KW, RIGAKU, TOKYO, JAPAN) with a wavelength of $\lambda = 0.15418$ nm over an angular range of $10° \leq 2\theta \leq 70°$ at a step width of 0.01 °. Raman spectroscopy was conducted with an ARAMIS from Horiba Jobin Yvon using argon ion laser excited at 514nm. The microstructure and morphology of the QWF electrodes were analyzed by scanning electron microscopy (SEM, XL30, Philips) at an acceleration voltage of 10 kV and transmission electron microscopy (TEM, Tecnai G2 F30 S-Twin, FEI) operated at 300 kV. The chemical composition of the QWF electrodes were characterized using elemental analysis (EA) and inductively conductive plasma (ICP) of the developed fabric electrodes. The carbon content in the electrodes was determined by EA (Flash 2000, Thermo Scientific). Metallic elements such as Al, Fe, and Ni were determined by ICP optical emission spectrometer (inductively coupled plasma testing machine, Thermo Scientific Co./iCAP 6300 Duo).

Electrochemical measurements: Electrochemical tests were carried out using a 2032 coin-type half-cell with Li metal as both the counter and reference electrodes. The coin cell batteries were assembled in an Ar-gas-filled glove box with H_2O content < 0.3 ppm and O_2 content < 0.1 ppm.

The electrolyte was prepared by dissolving 1 M $LiPF_6$ (99.99%, Aldrich) and a mixture of ethylene carbonate and ethyl-methyl carbonate (EC-EMC) at a volume ratio of 1:1 (Panaxetec, South Korea). The glass fiber membranes (GF/D, Whatman) were used as separators with a thickness of 1.55 mm. The galvanostatic measurements were carried out in a cut-off voltage potential range from 0.01 to 2.0 V (vs. Li/Li^+) using a battery cycler (WBCS3000, WonATech). For the rate capability tests, the charge-discharge rate was varied from 0.05 C to 1 C-rate at 25 °C in a constant-temperature convection oven. The theoretical capacity of graphite (372 mAh g^{-1}) was used to calculate the C-rate (372 mA g^{-1} = 1 C-rate). Electrochemical impedance spectroscopy (EIS) was performed between 100 MHz and 1MHz at the open circuit potential of the cell, which had a signal peak-to-peak amplitude of 5 mV performed by a multi-channel battery tester (BioLogic VMP3, France).

3. Results and Discussion

Material Synthesis

In case of using a quartz woven fabric, as a substrate, the important factors determining the energy efficiency of CNTs are to ensure uniformity of the distribution of CNTs grown on the fabric surface, mitigation of mutual interference through uniform vertical growth, and uniformity of height. CNTs, which were grown on the fabric substrate using the previous synthetic method, had inhomogeneous height because of the unevenness of the fabric surface, causing a problem of crossing with each other. In addition, as long-grown CNTs bend after growth, they become entangled or become a complex network structure. The morphology becomes an important factor affecting electrochemical performance when CNTs were used as an electrode material. Therefore, in this study, we studied a special method in which high-yield CNT can be grown vertically to an appropriate length that can minimize bending and deformation after growth via PECVD. Table 1 shows physical and mechanical properties of silica glass fibers in quartz woven fabric.

Table 1. The material properties of silica glass fibers in quartz woven fabric.

Filament Diameter	Specific Gravity	Tensile Strength	Tensile Modulus	CTE	Thermal Stability	Thermal Conductivity
μm	g cc^{-1}	GPa	GPa	m/(m·°C)	°C	W/(m·K)
9.0	2.2	3.4	69	5.4 * 10^{-7}	1200	0.0033

By changing the deposition of Al and Fe nanoparticles as a metal catalyst layer before CNTs were grown, we tried to confirm the possibility of improving the distribution of CNT forest and increasing the growth yield compared to pristine QWF (P-QWF). For electrode synthesis, a nanostructured electrode was fabricated via e-beam evaporator and PECVD. The fabrication of CNT-coated QWF electrode (C-QWF), was carried out in two sequential steps, inside and outside the CVD chamber. First, to fabricate nanostructured electrodes on fabric substrates, metal nanoparticles were deposited as a catalyst on a fabric substrate through a pre-treatment process using an e-beam evaporator before the plasma CVD process. For effective carbon nanotube growth, Fe and Al nanoparticles were deposited with a diameter within 1-10 nm. In the process of growing CNT on the fabric electrode, the reason for considering the metal catalyst is to increase the in-plane electrical conductivity when CNTs were grown in a vertical direction on the surface of QWF. Furthermore, this CNT structure not only has a role to overcome the low electrical conductivity of QWF but also can store the considerable lithium ions because of their large surface area.

In order to investigate the crystal structure of the QWF series, XRD was executed from 10 to 70° as shown in Figure 1a. The XRD peak of both QWF electrodes can be broadly indexed as amorphous silica, detected at 2θ = 20.63°, and as crystalline silica, which is detected at 2θ = 22.82°. The Raman spectra of the QWF electrodes confirm several shifts in the low wavenumber range from 100 to 700 cm^{-1}, related to amorphous silica. It was confirmed that the crystalline SiO_2 peak was observed in C-QWF

in XRD after heat treatment but disappeared in Raman spectra, as seen in Figure 1b. The change of Raman peak according to the heat treatment of SiO_2 is due to the difference in crystallinity according to the temperature of the silica, and it is also proof that the initial amorphous silica was crystallized by the heat treatment as CNTs grew. In terms of CNTs, the D band, located at 1350 cm^{-1}, is related to the size of the in-plane sp^2 domains, while the G band, located at 1600 cm^{-1}, arises from the first-order scattering of the E_{2g} phonon of the sp^2 C. The D/G band of the C-QWF electrode appeared after the growth of CNTs, indicating the formation of both the new graphitic domain and defect-induced disordered sp^2 carbon atoms. The increase of the D/G band ratio in the C-QWF electrode provides direct evidence for the growth of CNTs on the surface of silica fabric.

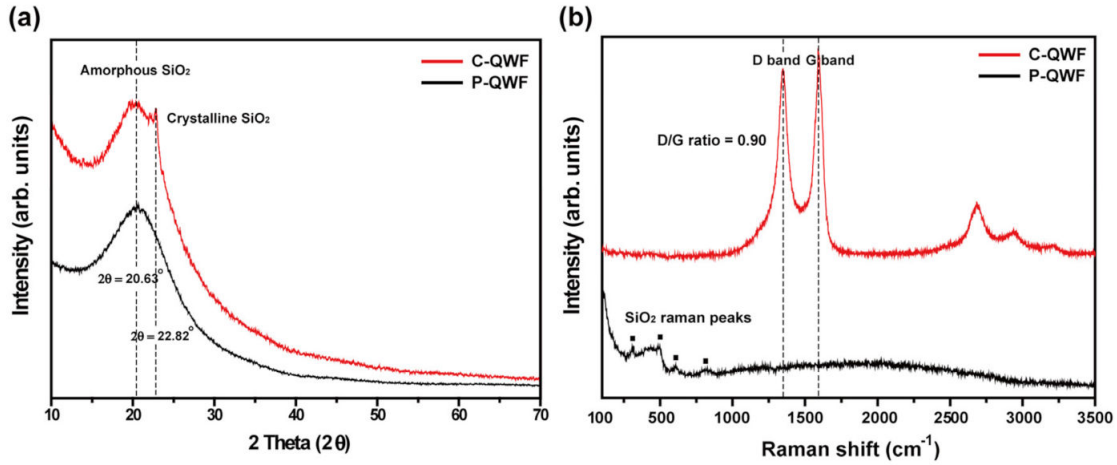

Figure 1. (**a**) X-ray powder diffraction patterns (10–70°) of the quartz woven fabric (QWF) electrodes; (**b**) Raman spectroscopy of the QWF electrodes.

Table 2 shows the compositional ratio of deposited metal catalysts contributing the growth of carbon layer and CNTs in C-QWF electrode. This was confirmed by ICP-MS and EA, respectively. The elemental ratio of metal catalysts confirm that the primary deposition effectively occurred on the silica surface through the sputtering process. The increase in weight ratio from P-QWF of 0.161% to C-QWF of 0.238% also shows that the metal catalysts effectively assist the growth of CNTs. The optical image and the morphology of the P-QWF electrode are shown in Figure 2a,b. Figure 2c shows the surface of silica fiber exists without other impurities before the CVD process. After the growth of CNTs on P-QWF, the color of the QWF electrode is changed from white to black due to the existence of CNTs, and its surface also looks rougher than before, as shown in Figure 2d,e. As-synthesized CNTs are observed entangled with each other on the surface in Figure 2f.

Table 2. The elemental composition of the QWF electrodes.

Samples	EA (%)	ICP (mg kg^{-1})		
	Carbon	Aluminum	Iron	Silicon
P-QWF	0.161	48.2	56.9	$4.85 * 10^5$
C-QWF	0.238	115	83.3	$4.96 * 10^5$

The microstructure and morphology of the QWF electrodes were observed using high-resolution transmission electron microscopy (HRTEM) as shown in Figure 3. Compared to the TEM images of the silica fiber in Figure 3a, the C-QWF homogenously spread throughout the silica fiber as shown in Figure 3b, similar to Figure 2f, and Fe nanoparticles as growth catalysts are more distinguishable. The crystallinity and phase of QWF electrodes were investigated by the selected area electron diffraction (SAED) patterns. Figure 3c shows the amorphous or very low crystalline phase of silica. In contrast, the SAED pattern of C-QWF electrode has various manifold spots, implying a poly-crystalline

environment of Fe nanoparticles. The ring pattern is computed as a function of the radial distance from the center of the diffraction pattern and described in the top right of Figure 3d.

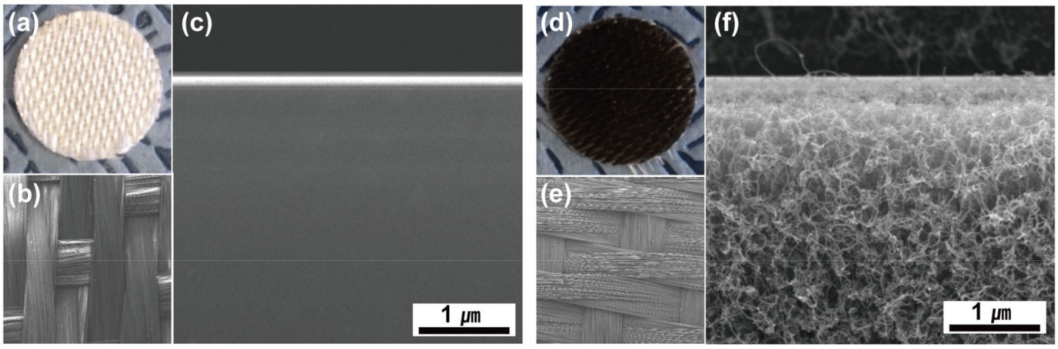

Figure 2. (**a**) Optical image of the pristine QWF (P-QWF) electrode. SEM images of the P-QWF electrode; (**b**) Top view at low magnification; (**c**) Cross-sectional view; (**d**) Optical image of the copper nanotube (CNT)-coated QWF electrode (C-QWF) electrode. SEM images of the C-QWF electrode; (**e**) Top view at low magnification; (**f**) Cross-sectional view.

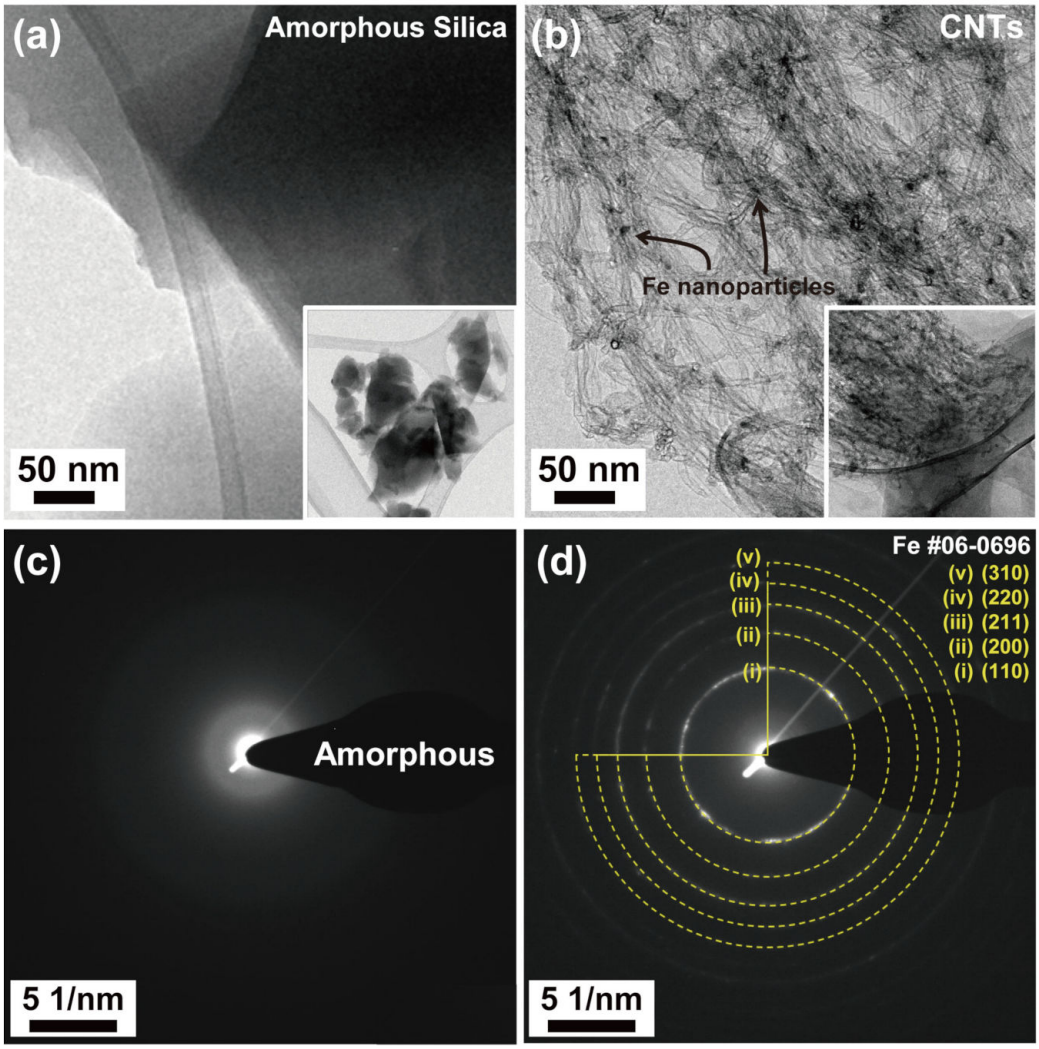

Figure 3. TEM images of the (**a**) P-QWF; (**b**) C-QWF and selected area electron diffraction (SAED) pattern of the (**c**) P-QWF and (**d**) C-QWF.

The electrochemical performances of the QWF electrodes are presented in Figure 4. The reversible capacity of P-QWF electrode is under 50 mAh g^{-1} because of the sluggish electrical conductivity of silica fiber. In the case of the C-QWF electrode, it had a discharge capacity of 640 mAh g^{-1} in the first cycle, and dropped to 485 mAh g^{-1} in the next cycle because of the formation of the solid electrolyte interphase (SEI) layer. It obtained the reversible capacity of 380 mAh g^{-1}, which is close to the theoretical capacity of graphite (372 mAh g^{-1}). This remarkable energy density is expected to be caused by a large surface area of entangled CNTs, facilitating the reaction site to store lithium ion and providing the electron path between the nonconductive substrate and external circuit without any current collector.

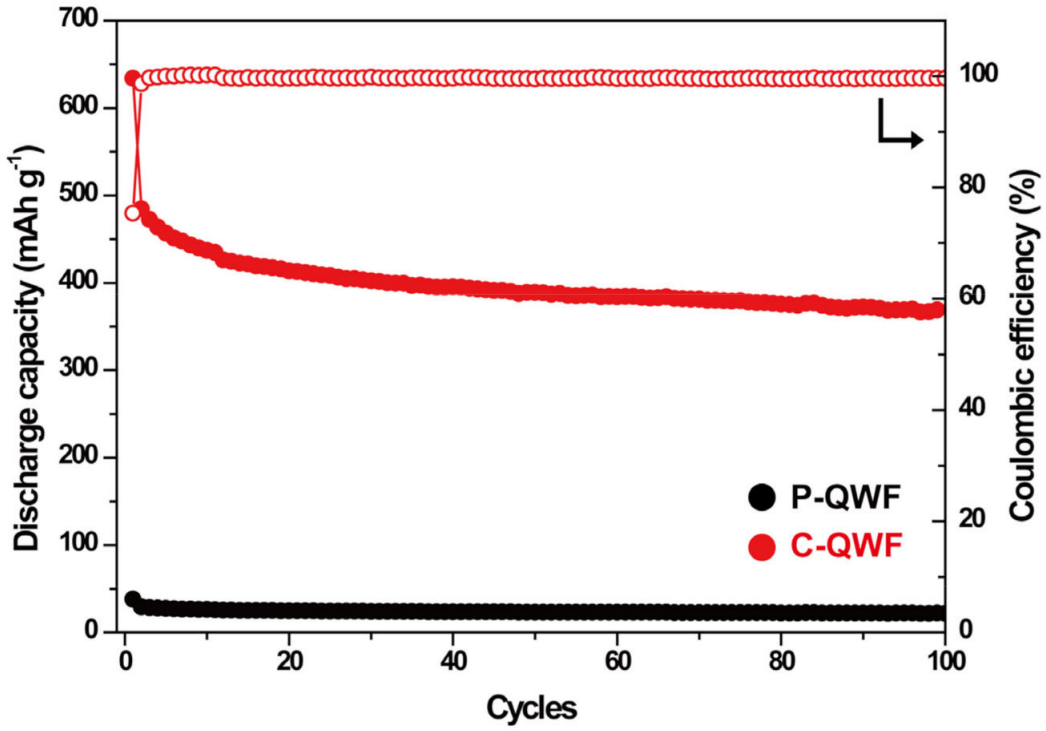

Figure 4. Cycle performances of QWF electrodes at a rate of 0.05 C-rate (red: C-QWF, black: P-QWF).

The rate performances of the C-QWF electrode are 660, 380, 298, 192, and 99 mAh g^{-1} at different current densities from 0.05 to 0.1, 0.2, 0.5, and 1.0 C-rate, respectively, as shown in Figure 5a. When the current was decreased to 0.1 C-rate, it still exhibited a reversible capacity of 369 mAh g^{-1}. This means that the C-QWF anode can tolerate high-rate cycling even at 1 C-rate, although the main composition of the electrodes is amorphous silicon oxide, which cannot provide electron paths. The voltage profiles in Figure 5b demonstrate the excellent electrochemical reversibility with a coulombic efficiency of 99.5%, except the first cycle. The plateau located at 0.7 V in the first lithiation process is generally known to originate from the formation of the SEI layer, relating to the decomposition of the organic electrolyte and irreversible reactions.

Usually, ohmic resistance (R_e) in the battery is equal to the intercept at the Z_{real} axis. The high-frequency semicircle is attributed to the resistance of the surface film (R_s), the medium-frequency semicircle reflects the charge-transfer resistance (R_{ct}), and the low-frequency tail could be considered as Warburg impedance, which is associated with Li-ion diffusion in the bulk of the electrode. As shown in Figure 6, the Nyquist plots of the QWF electrodes show a decrease of electrical conductivity according to the intercept at the Z_{real} axis, similar to the electrochemical performance of C-QWF electrodes. The resistance was measured by fitting the impedance spectrum with the equivalent model combining the diameters of the semicircles. The smaller intercept at the Z_{real} axis of the C-QWF (42.8 Ω cm^{-2}) than that of P-QWF (60.3 Ω cm^{-2}) indicates lower charge resistance. In view of these

results, the QWF electrode in which CNTs are grown can operate as an effective lithium storage structure and also serve as a support for an electrode material requiring structural stability. By establishing a high reversible capacity through C-QWF, it provides an effective and new perspective on the breakthrough of the limitations for conventional electrodes of LIBs.

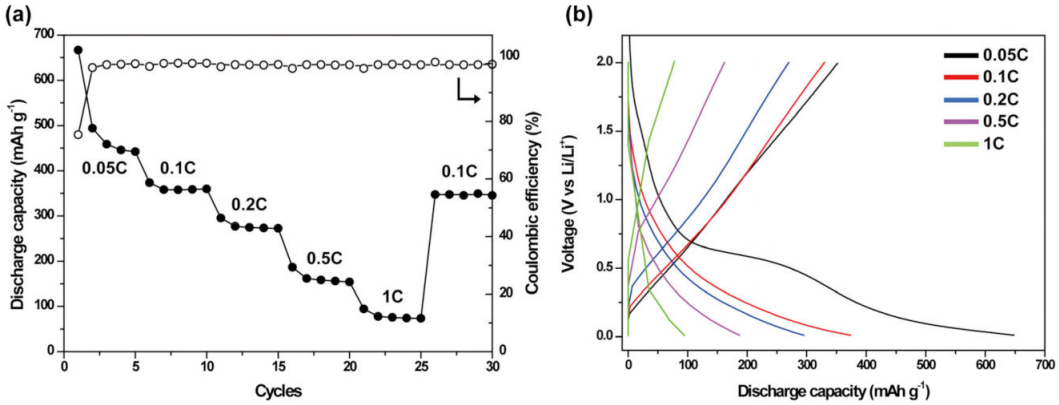

Figure 5. (**a**) Rate performance of the C-QWF electrode at a rate of 0.05 to 1 C-rate; (**b**) Galvanostatic discharge/charge voltage profiles of C-QWF between 0.01 and 2.00 V.

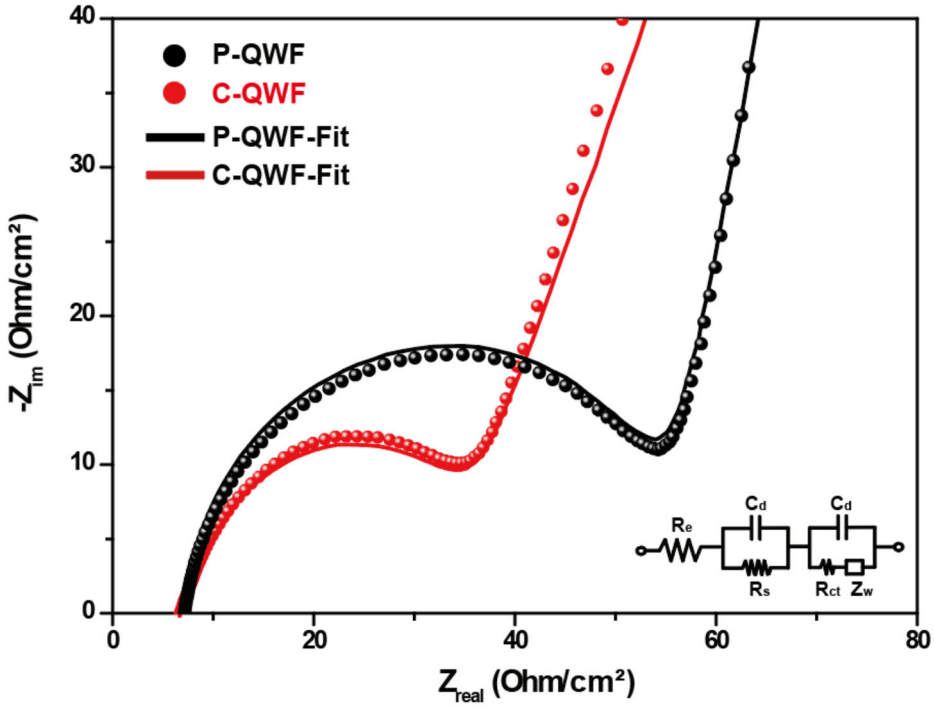

Figure 6. Nyquist plots of P-QWF (60.3 Ω cm^{-2}) and C-QWF electrodes (42.8 Ω cm^{-2}).

4. Conclusions

To make an effective lithium storage with a nano-tangled structure for a robust battery electrode, CNT was successfully grown on the QWF substrate via the sequential two-step deposition method. The C-QWF electrode exhibited a high energy density of 369 mAh g^{-1} at 0.1 C-rate after cycling with a Coulombic efficiency of 99.5%, which suggests that it can be a robust LIB with superior electrical and mechanical properties. It is closed to the theoretical capacity of CNTs (372 mAh g^{-1}), despite the fact that the electrode is mostly composed of silica and has a sluggish electrical conductivity. The benefits of this electrode are its facile synthesis for large-scale production, as well as an electrochemical performance

that features a specific reversible capacity of the C-QWF electrode for robust LIBs and approaches the level of being applied as a practical battery.

Author Contributions: Conceptualization, M.-Y.P., C.-G.K., and J.-H.K.; Methodology, M.-Y.P., and J.-H.K.; Investigation, M.-Y.P., and J.-H.K.; Writing—Original Draft, M.-Y.P., and J.-H.K.; Writing—Review & Editing, M.-Y.P., C.-G.K., and J.-H.K. All authors have read and agreed to the published version of the manuscript.

Funding: This research received no external funding.

Acknowledgments: The proposed works have been carried out in Korea Advanced Institute of Science and Technology and School of Materials Science and Engineering of Gyeongsang National University. The authors would also like to acknowledge C. K. L.

Conflicts of Interest: The authors declare no conflict of interest.

References

1. Kang, B.; Ceder, G. Battery materials for ultrafast charging and discharging. *Nature* **2009**, *458*, 190–193. [CrossRef]
2. Armand, M. Issues and challenges facing rechargeable lithium batteries. *Nature* **2001**, *414*, 359–367.
3. Armand, M.; Tarascon, J.-M. Building better batteries. *Nature* **2008**, *451*, 652–657. [CrossRef]
4. Larcher, D.; Tarascon, J.M. Towards greener and more sustainable batteries for electrical energy storage. *Nat. Chem.* **2015**, *7*, 19–29. [CrossRef] [PubMed]
5. Kjell, M.H.; Jacques, E.; Zenkert, D.; Behm, M.; Lindbergh, G. PAN-Based Carbon Fiber Negative Electrodes for Structural Lithium-Ion Batteries. *J. Electrochem. Soc.* **2011**, *158*, A1455. [CrossRef]
6. Lee, J.K.; An, K.W.; Ju, J.B.; Cho, B.W.; Cho, W.I.; Park, D.; Yun, K.S. Electrochemical properties of PAN-based carbon fibers as anodes for rechargeable lithium ion batteries. *Carbon N. Y.* **2001**, *39*, 1299–1305. [CrossRef]
7. Leijonmarck, S.; Carlson, T.; Lindbergh, G.; Asp, L.E.; Maples, H.; Bismarck, A. Solid polymer electrolyte-coated carbon fibres for structural and novel micro batteries. *Compos. Sci. Technol.* **2013**, *89*, 149–157. [CrossRef]
8. Li, J.; Ye, Q.; Cassell, A.; Ng, H.T.; Stevens, R.; Han, J.; Meyyappan, M. Bottom-up approach for carbon nanotube interconnects. *Appl. Phys. Lett.* **2003**, *82*, 2491–2493. [CrossRef]
9. Ryu, J.; Kim, S.W.; Kang, K.; Park, C.B. Synthesis of diphenylalanine/cobalt oxide hybrid nanowires and their application to energy storage. *ACS Nano* **2010**, *4*, 159–164. [CrossRef]
10. Gao, Y.; Adusumilli, S.P.; Turner, J.; Lesperance, L.; Westgate, C.; Sammakia, B. Factors affecting the growth of carbon nanofibers on titanium substrates and their electrical properties. *J. Nanosci. Nanotechnol.* **2012**, *12*, 7777–7787. [CrossRef]
11. Welna, D.T.; Qu, L.; Taylor, B.E.; Dai, L.; Durstock, M.F. Vertically aligned carbon nanotube electrodes for lithium-ion batteries. *J. Power Sources* **2011**, *196*, 1455–1460. [CrossRef]
12. Park, M.Y.; Kim, J.H.; Kim, D.K.; Kim, C.G. Perspective on Carbon Fiber Woven Fabric Electrodes for Structural Batteries. *Fibers Polym.* **2018**, *19*, 599–606. [CrossRef]
13. Park, S.; Dong-Won, P.; Yang, C.S.; Kim, K.R.; Kwak, J.H.; So, H.M.; Ahn, C.W.; Kim, B.S.; Chang, H.; Lee, J.O. Vertically aligned carbon nanotube electrodes directly grown on a glassy carbon electrode. *ACS Nano* **2011**, *5*, 7061–7068. [CrossRef] [PubMed]
14. Jost, K.; Perez, C.R.; McDonough, J.K.; Presser, V.; Heon, M.; Dion, G.; Gogotsi, Y. Carbon coated textiles for flexible energy storage. *Energy Environ. Sci.* **2011**, *4*, 5060–5067. [CrossRef]
15. Leela Mohana Reddy, A.; Estaline Amitha, F.; Jafri, I.; Ramaprabhu, S. Asymmetric flexible supercapacitor stack. *Nanoscale Res. Lett.* **2008**, *3*, 145–151. [CrossRef]
16. Qian, H.; Kucernak, A.R.; Greenhalgh, E.S.; Bismarck, A.; Shaffer, M.S.P. Multifunctional structural supercapacitor composites based on carbon aerogel modified high performance carbon fiber fabric. *ACS Appl. Mater. Interfaces* **2013**, *5*, 6113–6122. [CrossRef]
17. Behr, M.J.; Gaulding, E.A.; Mkhoyan, K.A.; Aydil, E.S. Effect of hydrogen on catalyst nanoparticles in carbon nanotube growth. *J. Appl. Phys.* **2010**, *108*, 053303. [CrossRef]
18. Delzeit, L.; Nguyen, C.V.; Chen, B.; Stevens, R.; Cassell, A.; Han, J.; Meyyappan, M. Multiwalled carbon nanotubes by chemical vapor deposition using multilayered metal catalysts. *J. Phys. Chem. B* **2002**, *106*, 5629–5635. [CrossRef]

19. Pamula, E.; Rouxhet, P.G. Bulk and surface chemical functionalities of type III PAN-based carbon fibres. *Carbon N. Y.* **2003**, *41*, 1905–1915. [CrossRef]
20. Shui, X.; Chung, D.D.L.; Frysz, C.A. Hairy carbon electrodes studied by cyclic voltammetry and battery discharge testing. *J. Power Sources* **1994**, *47*, 313–320. [CrossRef]